Design of HTS Excitation Coil for Homopolar Inductor Machine Considering Critical Current Reduction of Local Turn

Yuanhang Pan, Jiangtao Yang, Qing Li, Xuezhi Luo, Shoudao Huang, Chuang Gao, and Jun Ma

***Abstract*—The high temperature superconducting homopolar inductor machine (HTS-HIM) is identified as a promising candidate for the high-speed field of superconducting machine. The reliability and performance of HTS-HIM is closely related to the critical current of its HTS excitation coil. However, the critical current is limited by the turn with the highest risk of quench, which means that not all the turns of HTS coil can achieve the best performance. Targeting ensures the reliability of HTS-HIM and enhance the utilization rate of HTS tape, the HTS coil is designed considering the critical current reduction of local turn in this paper. Firstly, the operation principle of HTS-HIM is illustrated, and the design process is given. Then, the feasibility of calculating critical current using constant sweep rate method is described, and the HTS coil of a 10 kW HTS-HIM is designed utilizing the MAX criterion. Thirdly, the external field of the HTS coil is analyzed based on the simplified model of HTS-HIM. According to the external field distribution, an easily installed L-shaped flux diverter is proposed to suppress critical current reduction of local turn of HTS coil. The results show that the current safety margin is increased by 24 % at the cost of very little extra loss and weight through the proposed method.**

***Index Terms*—High temperature superconducting homopolar inductor machine (HTS-HIM), critical current, HTS coil design, flux diverter, superconducting machine.**

I. Introduction

Since the high temperature superconducting (HTS) machine has potential merits of high efficiency and high power density [1], [2], [3], the turbo-power superconducting system integrating liquid hydrogen energy refrigeration becomes the application trend of high power aviation all electrical system. Compared to the conventional machine topologies, the structures suitable for high-speed operation are more favored in the aviation field. The HTS-HIM that can operate at extremely high speed due to its robust rotor structure attracts wide attention in the field of high-speed superconducting machines [4], [5].

The research on HTS-HIM has been going on for a long time. Several studies have proposed the conceptual design of HTS-HIM for pursuing high power density [6], [7], [8]. Those work focused on improving the efficiency and reduce the weight of the system. To further improve the power density, it is necessary to carry out research on achieving high speed operation of HTS-HIM. In [9], an HTS-HIM for aerospace application was designed and analyzed, whose speed reaches 25000 rpm. In [10], a 1.3 MW, 10000 rpm HTS-HIM for aviation applications was designed and manufactured. Then a bearingless HTS-HIM for flywheel energy storage systems was proposed to improve the efficiency in [11], whose rated speed and efficiency are 60000 rpm and 87 %, respectively. On the other hand, to take fully use of rotor structure and improve excitation capacity, the permanent magnet was arranged at the rotor slot of HTS-HIM in [12]. In addition, the loss of HTS-HIM attracts attention as well. The temperature distribution of a 500 kW HTS-HIM and the heat caused by ripple field are analyzed in [13]. The loss generated in the HTS coil inside HTS-HIM is focused on in [14]. However, it can be found that there is a lack of research on the design of the HTS coil in HTS-HIM.

In the design of HTS-HIM, it is necessary to determine the rated excitation current according to the critical current of HTS coil. However, due to the anisotropy of HTS REBCO coated conductors, the turns of one HTS coil in different external fields have different critical currents. To prevent thermal runaway quench from damaging the HTS coil, some studies determined the critical current utilizing more sensitive criterion [15], [16], [17]. The main idea is that the critical current of the turn with the highest risk of quench (in the strongest external field) is supposed to be taken as the critical current of HTS coil. This means that the rated excitation current is much smaller than their critical currents for most of the turns, which causes that the performance of the HTS coil cannot be fully exploited. It is unacceptable for the pursuit of high efficiency and high power density. Thus, it is necessary to take measures to suppress the critical current reduction of local turn due to the field aggregation. The common method is to change the distribution of the external magnetic field. A raised-edge flux diverter was proposed to enhance the maximum critical current and energy storage capacity of solenoid coil simultaneously in [18]. The notch-shaped flux

This work was supported in part by the National Natural Science Foundation of China under Grant 52007055, and in part by the Youth Cultivation Fund of Chinese Academy of Sciences under Grant E224821231. *(Corresponding author: Jiangtao Yang).*

Yuanhang Pan, Jiangtao Yang, Qing Li, Xuezhi Luo, and Shoudao Huang are with the College of Electrical and Information Engineering, Hunan University, Changsha 410082, China (e-mail: yangjiangtao@hnu.edu.cn).

Chuang Gao is with the Shanghai Advanced Research Institute, Chinese Academy of Sciences, Shanghai 201210, China.

Jun Ma is with the Electrical Energy Management Group (EEMG), School of Electrical, Electronic and Mechanical Engineering, University of Bristol, Bristol, UK.

diverter was proved to be able to increase the critical current of the HTS coil more than the simple-shaped one in [19]. The field ripple was weakened through introducing copper shield and flux diverter into the cryostat in [20]. However, most of the above studies are based on individual HTS coil system. For the HTS-HIM, its critical current is significantly lower than that of an individual HTS coil due to the presence of iron core [21]. Besides, the field of excitation window is complicated [22], so the structure of HTS-HIM needs to be considered to suppress the critical current reduction of local turn. Further, the suppression measure taken cannot affect the output performance.

In this paper, the HTS coil of a 10 kW HTS-HIM is designed considering critical current reduction of local turn, aiming to enhance the reliability of HTS-HIM. To suppress the critical current reduction of local turn, the external field of HTS coil in HTS-HIM is analyzed from two perspectives of the machine and HTS coil. Based on this, an L-shaped flux diverter is proposed and analyzed. The rest part of this article is organized as follows. In Section II, the topology and design process of the HTS-HIM are illustrated. In Section III, considering the critical current reduction of local turn, the HTS coil is designed utilizing MAX criterion and constant sweep rate method. In Section IV, based on the external field distribution of HTS coil, an L-shaped flux diverter is proposed to suppress the critical current reduction of local turn. Finally, the conclusions of this paper are drawn.

II. Topology and Design Process

A. Topology of HTS-HIM

The schematic structural diagram of HTS-HIM is depicted in Fig. 1. Compared with the conventional HIM, the copper excitation winding is replaced by HTS coil in the HTS-HIM. The HTS coil and copper armature winding are located on the stator, which achieves static cooling and ensures the reliability of HTS-HIM operation. To avoid stator tooth core saturation and eliminate the tooth-tip harmonic, the air-gap armature winding is adopted. The rotor is forged from high strength alloy steel, which consists of salient poles on both sides of the rotor and a solid cylinder in the middle. Since there are no appurtenances on solid rotor, the HTS-HIM can operate at extremely high speed, which means that the application of superconducting machine in the field of high-speed is expected to be realized through HTS-HIM.

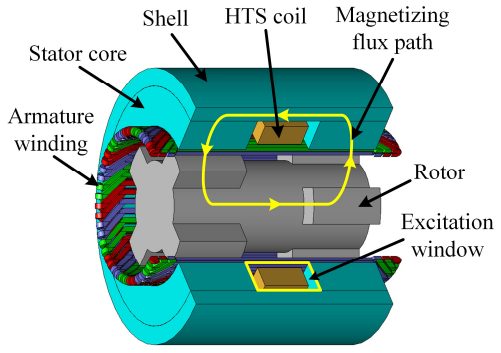

Fig. 1. The topology of HTS-HIM.

B. Design Process of HTS-HIM

The design flowchart of HTS-HIM is described in Fig. 2. Compared with conventional HIM design, it is necessary to pay attention to the coupling between machine and HTS coil in the design of HTS-HIM. As designing from the perspective of machine, the HTS coil is regarded as a conductor with infinite conductivity. In other words, in electromagnetic (EM) design of HTS-HIM, only the magnetomotive force (MMF) generated by HTS coil is considered. It should be noted that the space must be reserved in excitation window to install the cryostat and HTS coil support. For the design of HTS coil, it is necessary to determine the size of HTS coil according to the parameters of EM design. Moreover, accurate calculation of critical current is crucial to ensure the reliable operation of HTS-HIM. The detailed process of EM design of HIM is given in [4]. The design of HTS coil is based on the excitation MMF and excitation window size that are obtained from EM design. The initial parameters of the 10 kW HTS-HIM after EM design are listed in Table I.

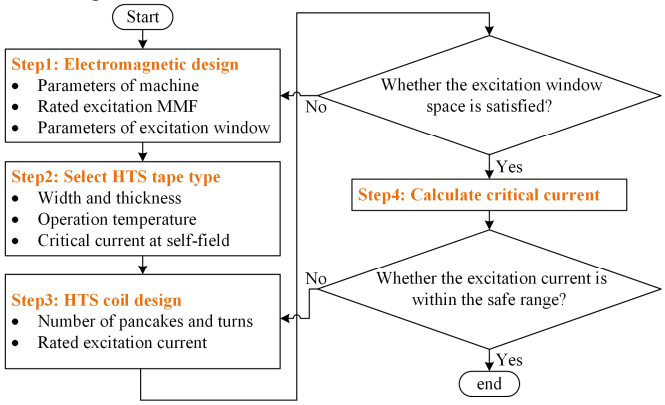

Fig. 2. Design flowchart of HTS-HIM.

TABLE I
Initial Parameters of HTS-HIM

Item	Value	Item	Value
Electrical power (kW)	10	Rated speed (r/min)	3000
Rated phase voltage (V)	250	Rotor tooth width (°)	30
Outer diameter of shell (mm)	302	Rotor slot depth (mm)	25
Inner diameter of shell (mm)	278	Total length (mm)	209
Inner diameter of stator (mm)	174	Pole-pairs	4
Air-gap length (mm)	7	No. of stator slots	48
One stator core length (mm)	67	Parallel branches	2
Rated MMF (AT)	19296	Width of EW (mm)	75
Height of EW (mm)	52		

TABLE II
Parameters of HTS Tape

Item	Value
Material	REBCO
Tape width (mm)	12
Tape thickness (mm)	0.5
Layer width (mm)	10
Layer thickness (mm)	0.001
Operating temperature (K)	75

III. Design of HTS Coil

A. FEA Model of HTS Coil

To pursue higher current carrying capacity, the ring-shaped

HTS coil is wound using second-generation HTS REBCO tape manufactured by Shanghai Superconductor. The parameters of the HTS tape are shown in Table II, where the tape thickness includes insulation thickness between turns. To satisfy the requirements of HTS-HIM, the operating temperature of HTS coil is 75 K, cooled by liquid nitrogen. Moreover, limited by manufacturing technology and cost, the HTS coil adopts the structure with multiple pancakes. Fig. 3 shows the structure of the quadruple-pancake ring-shaped HTS coil in HTS-HIM, where w is the gap between pancakes and n is the number of turns per pancake.

For second-generation HTS tape, based on the thin strip approximation, ***T-A*** formulation is used to establish the finite element analysis (FEA) model [23], [24], [25], where $\boldsymbol{T}$ is current vector potential, and $\boldsymbol{A}$ is magnetic vector potential. The two-dimensional (2D) axisymmetric model is used to analyze the ring-shaped HTS coil. The governing equations of $\boldsymbol{T}$ and $\boldsymbol{A}$ in cylindrical coordinate system are expressed as,

$$\frac{\partial}{\partial z}\left(\rho\frac{\partial T_r}{\partial z}\right)=\frac{\partial B_r}{\partial t}, \tag{1}$$

$$\nabla\times\left(\nabla\times A_\varphi\right)=\mu\cdot J_\varphi, \tag{2}$$

where the subscripts r and φ indicate the components of each physical quantity in the corresponding direction, and ρ is the nonlinear resistivity of superconductor (SC), denoted by,

$$\rho=\frac{E_c}{J_c(\boldsymbol{B})}\left|\frac{\boldsymbol{J}}{J_c(\boldsymbol{B})}\right|^{n(\boldsymbol{B})-1}, \tag{3}$$

where E_c is the quench electric field criterion, which is usually taken as 1×10^{-4} V/m, and $J_c(\boldsymbol{B})$ and $n(\boldsymbol{B})$ reflect the effect of external magnetic field on the characteristics of the SC. In this work, the filed dependence of the critical current and n-value is obtained from the manufacture's material parameters shown in Fig. 4. As the magnetic field is perpendicular to the wide surface of the tape, the angle is 0 deg. The data shown in Fig. 4 are imported into to FEA software as interpolation functions to achieve anisotropy of the HTS tape, which avoids the extra work introduced by data fitting.

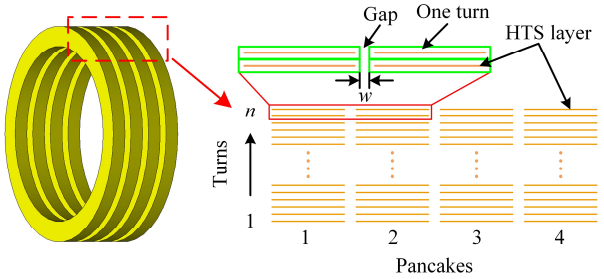

Fig. 3. Diagram of multiple pancakes ring-shaped HTS coil in HTS-HIM.

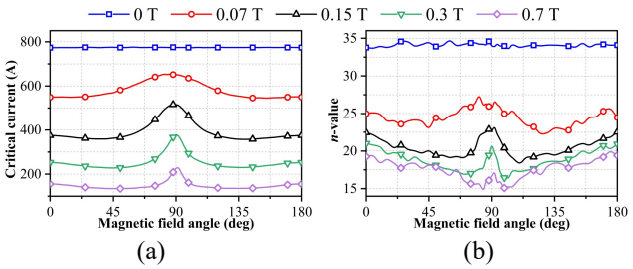

Fig. 4. Field dependence of HTS tape at 75 K [26]. (a) Critical current vs magnetic field angle. (b) n-value vs magnetic field angle.

B. Method of Calculating Critical Current

The accurate calculation of critical current plays a crucial role in determining the rated excitation current of HTS-HIM, which directly affects its reliability and output performance [27]. For an individual HTS coil, the perpendicular magnetic field is the largest at the two ends and the field is concentrated close to the inner turn [15], [18]. Therefore, the critical current of local turn reduces due to the uneven distribution of the external field. At the design stage, there are two criterion methods to calculate the critical current of the HTS coil [16]:

1) MAX criterion: I_{cM} is the current at which at least one turn of HTS coil meets $E_i/E_c = 1$. E_i is the average electric field of one turn, expressed as,

$$E_i=\iint_S \rho J_\varphi \mathrm{d}S \Big/ \iint_S \mathrm{d}S, \tag{4}$$

where S is the cross-section of one turn, and J_φ is the transport current density of the ring-shaped HTS coil in cylindrical coordinate system.

2) SUM criterion: I_{cS} is the current at which the average electric field E_{coil} of HTS coil meets $E_{coil}/E_c = 1$. E_{coil} is expressed as,

$$E_{coil}=\sum_i^N \int_l E_i \mathrm{d}l \Big/ L, \tag{5}$$

where N is the number of turns of HTS coil, and L is the total length of the HTS tape.

It can be seen that I_{cS} reflecting the average critical current level of all turns is the ideal critical current of HTS coil, while I_{cM} is the actual critical current that depends on the turn with the highest risk of quench. In addition, in the FEA, both E_i and E_{coil} directly reflect the relationship between resistivity and transport current of SC, excluding the induced electric field. Since only the voltage between the terminals of HTS coil can be measured in experimental, the SUM criterion is usually used to estimate the critical current [15]. In addition, a suitable calculation method can not only ensure the accuracy but also save the computation time. Corresponding to the experimental process, there are two methods to calculate the critical current in FEA:

1) Ramp-and-hold method (RAHM): The transport current is kept constant for a period of time after rising from one setpoint to another. Judge whether the E_{coil} at the end of the constant current period meets critical electric field criterion.

2) Constant sweep rate method (CSRM): The transport current rises at a constant sweep rate. Judge whether the E_{coil} meets the critical electric field criterion during current rise.

Comparing the two methods, the RAHM requires setting multiple current setpoints, so it is accurate but inefficient, while the CSRM is more efficient, but the screening current generated during the current rise affects the result. It is obvious that using CSRM to calculate the critical current is beneficial to improve the efficiency of HTS coil design. To analyze the calculation error of CSRM, a 100-turn double-pancake HTS coil is taken as an example, whose inner

diameter is 198 mm and operating temperature is 77 K. Its critical current calculated through RAHM and CSRM is 206.5 A and 207.4 A, respectively.

Fig. 5 gives the normalized electric field E_{coil}/E_c of the HTS coil with the transport current rising at a rate of 1 A/s to 207.4 A that is the critical current calculated by CSRM and then maintained at this value. It can be found that the inflection points of the current and the normalized electric field appear at the same time. After the current remains constant, E_{coil}/E_c gradually becomes stable. For the researched HTS coil, its normalized electric field at stability is greater than that at the inflection point. Since the exponential relationship between current density and electric field of HTS coil, the calculated critical current error is almost negligible using CSRM.

Fig. 6 shows the influence of different sweep rates on the calculation results using CSRM. The normalized electric field curve has an obvious tip as the current sweep rate is 20 A/s. As using the FEA software to calculate the critical current using CSRM, the termination condition is that $E_{coil}/E_c \geq 1$, and the current at the last step is the obtained critical current. Thus, in this case, the calculated critical current is 192 A, which is smaller than the actual value. Therefore, if the sweep rate is too large, the critical current calculated through the CSRM is small, which leads to the performance of HTS coil is not fully exploited. Moreover, the smaller the step size of output, the more accurate the calculation result using CRSM. It is a good choice to calculate the critical current of HTS coil using CRSM with a current sweep rate of 1 A/s and a step size of 0.1 s, which is beneficial to improve the design efficiency of HTS coil.

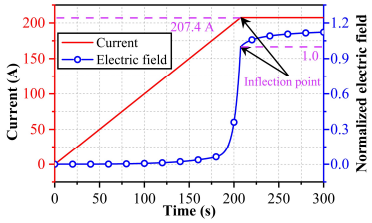

Fig. 5. The normalized electric field of the HTS coil when the transport current of HTS coil increases to 207.4 A and maintained at this value.

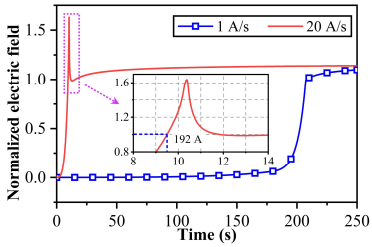

Fig. 6. The normalized electric field of HTS coil with different current sweep rates.

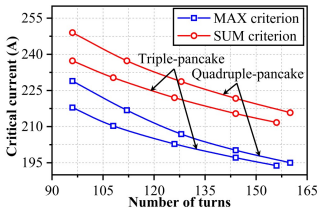

(a)

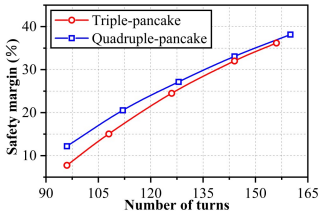

(b)

Fig. 7. The influence of number of pancakes on HTS coil. (a) Critical current vs No. of turns. (b) Safety margin vs No. of turns.

C. Excitation Current and Number of Turns

To improve the design efficiency, the HTS coil is optimized without the effect of iron core and CSRM is used. The initial excitation window size and rated excitation MMF have been obtained in EM design. Taking into account assembly space, the inner diameter of HTS coil is 208 mm. The influence of number of pancakes and turns on critical current is shown in Fig. 7(a). It shows that the critical current decreases as the number of turns increases. At the same number of turns, the critical current of the quadruple-pancake HTS coil is greater than that of the triple-pancake. The reason is that there are more turns affected by large perpendicular magnetic field at the both ends of triple-pancake HTS coil. In addition, actual critical current I_{cM} is much smaller than ideal critical current I_{cS}. As mentioned above, aggregated distribution of external field causes the critical current of certain turns of HTS coil to reduce. To ensure the safety of HTS coil, the smallest critical current among all turns should be taken as the critical current of HTS coil, which means that the MAX criterion is supposed to be used as the quench criterion for calculating its critical current in the process of designing HTS coil through FEA. The reason is that once the turns that have the smallest critical current are quenched, the HTS coil will be thermal runaway.

The determination of the excitation current is supposed to retain an appropriate safety margin. The current safety margin is defined as,

$$\gamma = (I_c - I_r)/I_c \times 100\%, \tag{6}$$

where γ is the current margin safety margin, which usually is 30 % in the design of HTS coil, I_r is the excitation current, and I_c is the critical current. The relationship between current safety margin and number of turns are presented in Fig. 7(b). Since the excitation current is inversely proportional to the number of turns, the current safety margin and the number of turns change the same trend. In addition, the safety margin of the quadruple-pancake HTS coil is greater than that of the triple-pancake, and the smaller the number of turns, the greater the difference. As the primary concern is safety of HTS coil, the number of pancakes and turns is 4 and 144, respectively.

Fig. 8(a) gives I_{cM} and I_{cS} of the quadruple-pancake HTS coil with different gap between pancakes, where the gap equal to 0 is an ideal case. The relative difference δ between I_{cS} and I_{cM} is given in Fig. 8(b), which is defined as,

$$\delta = (I_{cS} - I_{cM})/I_{cS} \times 100\%. \tag{7}$$

It can be seen that the uneven distribution of the field leads to a large difference between I_{cS} and I_{cM}, and δ reflects the level of critical current reduction. The larger δ, the more serious the critical current reduction, which is harmful to improve power density of the HTS-HIM. The results in Fig. 8 show that the larger the gap between pancakes, the larger the critical current, but also the larger δ. It is a contradiction in determining gap between pancakes. After comprehensive consideration, the gap is determined to be 2 mm.

With or without considering the critical current reduction of local turn, the critical currents of the optimized HTS coil are 200.2 A and 221.7 A in the absence of iron core, respectively. Considering the critical current reduction of local turn, the parameters of optimized HTS coil are obtained shown in Table III.

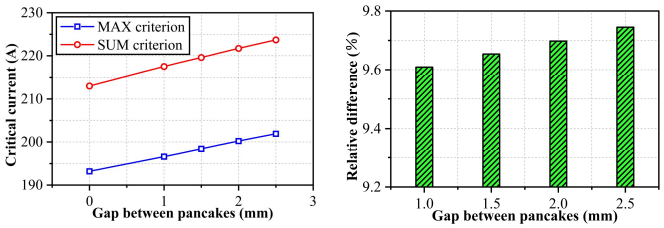

Fig. 8. The effect of gap between pancakes on critical current of HTS coil. (a) Critical current vs gap between pancakes. (b) Relative difference vs gap between pancakes.

TABLE III
PARAMETERS OF OPTIMIZED HTS COIL

Item	Value
Inner diameter (mm)	208
Outer diameter (mm)	244
No. of pancakes	4
No. of turns per pancake	36
Thickness (mm)	18
Width (mm)	54
Gap between pancakes (mm)	2
Rated excitation current (A)	134
Operating temperature (K)	75
Critical current (A)	200.2

IV. METHOD TO SUPPRESS CRITICAL CURRENT REDUCTION OF LOCAL TURN

Considering the critical current reduction of local turn, the parameters of HTS coil of the 10 kW are obtained. It can be found that there is a large difference between the ideal critical current and the actual critical current. The excitation current obtained with actual critical current as reference makes most of the turns unable to fully perform. Thus, the suppression of the critical current reduction of local turn is crucial.

A. Field Analysis of Excitation Window

The combine burden from three-dimensional nonlinearity HTS-HIM model and moving mesh makes FEA complex and time-consuming [28]. To improve the design and analysis efficiency of HTS-HIM, the three-dimensional FEA model is simplified into a 2D axisymmetric model. The machine model is simplified through introducing the carter coefficient [22], [29]. The simplified schematic diagram of the HTS-HIM with air-gap armature winding is shown in Fig. 9. Primarily, the initial model is simplified to a slotless model. Further, the slotless model is equivalent to a 2D axisymmetric model. The equivalent air-gap length of slotless model is expressed as,

$$\delta_{eq} = k_{cr}\delta, \tag{8}$$

where δ_{eq} is the equivalent air-gap length, δ is the initial physical air-gap length, and k_{cr} is the carter coefficient of rotor side, expressed as,

$$k_{cr} = B_{max} / B_{avg}, \tag{9}$$

where B_{max} is the amplitude of the magnetic flux density of one side of the air-gap, and B_{avg} is the average magnetic flux density of the corresponding air-gap. Finally, the direct coupling between HTS coil and non-superconducting region is realized when the HTS-HIM is stationary through mix ***T-A*** formulation: the ***T*** for HTS coil region and ***A*** for universe region [30].

The HTS coil of HTS-HIM located in excitation window interacts with the machine through magnetic field. As shown in Fig. 10(a), there are slot leakage flux and tooth leakage flux flowing through the HTS coil in the excitation window [22]. In addition, as can be seen from Fig. 10(b), the external field of HTS coil is evenly distributed along the circumference. The flux density near the rotor is obviously greater than that near the shell. Figs. 10(c) and (d) show the distributions of parallel and perpendicular magnetic fields, where the negative sign indicates that the direction of the magnetic field is opposite to the positive direction. It can be seen that the distribution of magnetic field is uneven. For parallel field, the closer to rotor, the greater the field. For perpendicular field, the maximum value occurs on both ends, and the values show a symmetric relationship. Since the critical current decreases significantly with the increase of external field, as shown in Fig. 4, it can be predicted that the innermost turns on both ends of HTS coil have the smallest critical current, and the critical current difference between inner turns and outer turns is huge.

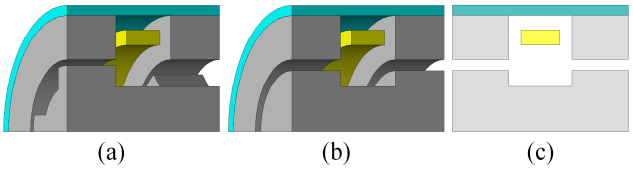

Fig. 9. The simplified schematic diagram of the HTS-HIM with air-gap armature winding. (a) Initial model. (b) Slotless model. (c) 2D axisymmetric model.

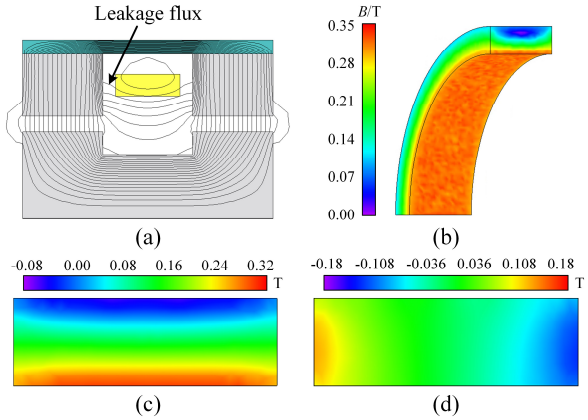

Fig. 10. The external magnetic field of HTS coil in excitation window. (a) Leakage flux. (b) Magnetic flux density distribution. (c) Parallel magnetic field. (d) Perpendicular magnetic field.

B. Critical Current of Each Turn

Fig. 11 presents the field distributions in two cases as the excitation current is 134 A, i) individual HTS coil and ii) HTS

coil in HTS-HIM. Due to the effect of iron core, the magnetic field distribution is obviously different in the two cases, which leads to the different in their critical currents. The I_{cM} of case-2 is 189.2 A and δ is 10.2 %, while the case-1 is 200.2 A and 9.7 %, respectively. It is obvious that the critical current of HTS coil in HTS-HIM is less than that of individual HTS coil since the presence of iron core. Besides, the critical current reduction of local turn is more serious. For simplicity, the following HTS coil represents the HTS coil in HTS-HIM.

As shown in Fig. 11(b), the flux path is changed since the presence of iron core, and the white circle area has the densest flux line. In addition, each turn of the HTS coil is in the self-field and the external field generated by the rest of turns. Each turn is numbered in the form (Pancakes, Turns), as shown in Fig. 3. The external field of HTS coil presents a symmetrical distribution, so only the critical currents of the pancake-1 and pancake-2 are analyzed.

As the transport current is 189.2 A that is the critical current of HTS coil, the normalized electric field and current density of each turn are show in Table IV. Obviously, (1, 1) has the smallest critical current, which is consistent with the analysis from the perspective of magnetic field. The turn with highest critical current is located near (2, 30). Once the current exceeds the critical current of (1, 1), it will be quenched and become a heat source, causing thermal runaway throughout the HTS coil. Therefore, (1, 1) limits the critical current of HTS coil, further causing the excitation current to be limited. The turns like (2, 30) cannot be fully utilized, which causes the waste of HTS tape and is not conducive to improve the power density.

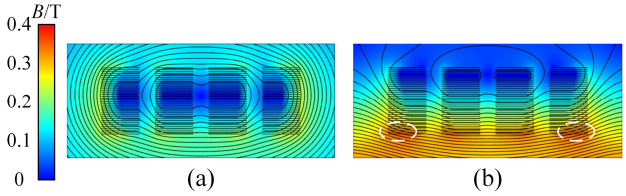

Fig. 11. The influence of iron core on external magnetic field. (a) Individual HTS coil. (b) HTS coil in HTS-HIM.

TABLE IV
STATE OF EACH TURN WITH CURRENT IS 189.2 A

No.	E_i/E_c	$J_\varphi/J_c(\boldsymbol{B})$	No.	E_i/E_c	$J_\varphi/J_c(\boldsymbol{B})$
(1, 1)	**1.184**	**1.010**	(2, 1)	0.0440	0.834
(1, 2)	0.797	0.986	(2, 2)	0.0344	0.824
(1, 5)	0.299	0.932	(2, 5)	0.0162	0.790
(1, 10)	0.0733	0.862	(2, 10)	0.00257	0.715
(1, 15)	0.00452	0.745	(2, 15)	0.00106	0.608
(1, 20)	0.00289	0.656	(2, 20)	0.00058	0.503
(1, 25)	0.00230	0.560	(2, 25)	0.000308	0.404
(1, 30)	0.00175	0.493	**(2, 30)**	**0.000214**	**0.367**
(1, 36)	0.00151	0.545	(2, 36)	0.000241	0.451

C. L-shaped Flux Diverter

The principle of suppressing critical current reduction of HTS coil is to change the external field distribution of the turn with greatest risk of quench. Since the perpendicular magnetic field has much greater effect on the critical current than the parallel magnetic field, the main idea is to change the flux path so that it is parallel to the turns by using soft magnetic material that has convergent effect on flux. Through analyzing the external field of HTS coil from two perspectives, it is found that (1, 1) has the smallest critical current. Based on the distribution of external field of HTS coil in HTS-HIM, an L-shaped flux diverter is proposed to suppress critical current reduction of local turn, as shown in Fig. 12. Its structure is simple and easy to install. The L-shaped flux diverter is made of Fe-Co-V soft magnetic alloy whose saturation magnetic flux density can reach 2.4 T. The thickness of the flux diverter is 2 mm. Allowing for installation and cooling of HTS coil, there is 2 mm gap between the HTS coil and flux diverter.

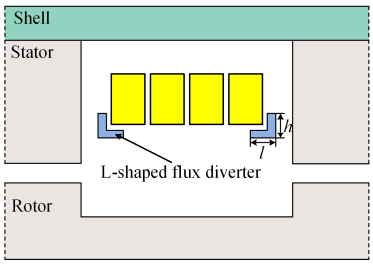

Fig. 12. The topology of L-shaped flux diverter. l and h are the length and height of the flux diverter, respectively.

TABLE V
EFFECT OF FLUX DIVERTER WITH DIFFERENT PARAMETERS

l (mm)	h (mm)	I_{cS} (A)	I_{cM} (A)	δ (%)	γ (%)
0	**0**	**210.7**	**189.2**	**10.20**	**29.18**
2	2	211.8	190.3	10.15	29.58
2	8	214.2	192.1	10.32	30.24
4	4	217.7	197.5	9.28	32.15
4	5	219.0	199.1	8.77	32.90
5	2	218.9	199.7	8.77	32.90
5	**5**	**224.7**	**210.0**	**6.54**	**36.19**
5	8	228.8	210.5	8.00	36.34
8	4	222.9	203.6	8.66	34.18
8	8	232.1	209.9	9.56	36.16

The effect of structure parameters on the suppressing ability of L-shape flux diverter is listed in Table V. The length and width equal to 0 represents the initial structural without the L-shaped flux diverter. The results show that when the height of the flux diverter reaches a certain value, its suppressing ability tends to saturation. The reason is that the turn that determines the critical current of the HTS coil is inside, and although increasing the height can improve the critical current of outside turns, it cannot increase the critical current of HTS coil. With increase of the length of flux diverter, it tends to be magnetically saturated, so suppressing ability is not significantly improved, on the contrary, the iron loss increases. Thus, under the premise of ensuring the performance, considering the suppressing ability, the length and height of L-shaped flux diverter are 5 mm, and the weight is 0.125 kg.

Compared with the initial structure, the critical current of the improved structure increases from 189.2 A to 210 A, and the current safety margin is increased by 24 %. More importantly, the relative difference δ between I_{cM} and I_{cS} is reduced by 35.9 %. Table VI lists the state of each turn with the current is 210 A in improved structure. Compared with the data in Table IV, the critical current of each turn is more even. Fig. 13 presents the critical currents of innermost 10 turns of the initial and improved structures. It can be seen that the critical currents of

turns of pancake-1 are greatly increase in the improved structure. Besides, compared with the initial structure, the critical current difference between turns decreases. While the critical currents of turns of pancakes-2 are almost the same in the two structures. The distributions of parallel and perpendicular magnetic fields in the improved structure as the transport current is 134 A are shown in Fig. 14.

TABLE VI
STATE OF EACH TURN IN IMPROVED STRUCTURE WITH CURRENT IS 210 A

No.	E_i/E_c	$J_\varphi/J_c(\boldsymbol{B})$	No.	E_i/E_c	$J_\varphi/J_c(\boldsymbol{B})$
(1, 1)	**1.220**	**1.012**	(2, 1)	1.182	1.010
(1, 2)	1.189	1.010	(2, 2)	0.838	0.990
(1, 5)	0.753	0.983	(2, 5)	0.311	0.934
(1, 10)	0.348	0.942	(2, 10)	0.0707	0.859
(1, 15)	0.0323	0.830	(2, 15)	0.00207	0.715
(1, 20)	0.00349	0.719	(2, 20)	0.00105	0.582
(1, 25)	0.00323	0.620	(2, 25)	0.000532	0.454
(1, 30)	0.00282	0.568	**(2, 30)**	**0.000386**	**0.425**
(1, 36)	0.00267	0.651	(2, 36)	0.000450	0.541

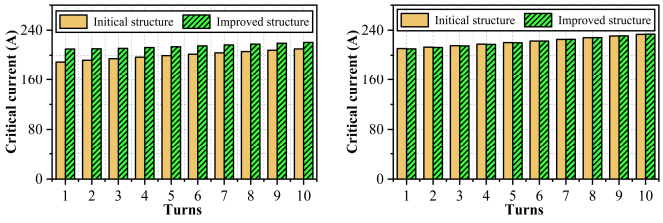

Fig. 13. The critical currents of innermost 10 turns in the two structures. (a) Pancake-1. (b) Pancake-2.

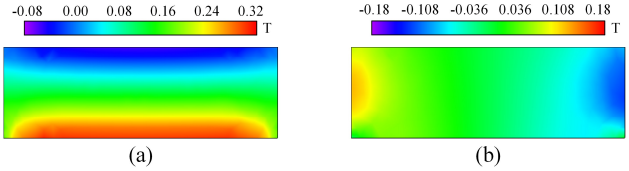

Fig. 14. The external field distribution of HTS coil in improved structure with transport current is 134 A. (a) Parallel magnetic field. (b) Perpendicular magnetic field.

D. Output Performance of HTS-HIM

The no-load air-gap magnetic flux densities of initial and improved structures are presented in Fig. 15. It can be seen that the air-gap magnetic flux density waveforms of two structures are almost the same, which means that the introduction of L-shaped flux diverter does not affect the output performance of the HTS-HIM. Fig. 16(a) shows the waveform of three-phase no-load back electromotive force (back-EMF), whose root mean square value is 252 V. The total voltage harmonic distortion is 6.8 %. In generating operation, the rated three-phase resistance is 18 Ω. The voltage spectrums of the two structures under the rated load condition are illustrated in Fig. 16(b). It can be found that the field generated by the eddy current of the L-shaped flux diverter has almost no effect on the output. In this case, the flux density distribution of the flux diverter is depicted in Fig. 17. The iron loss of the L-shaped flux diverter is 0.082 W: eddy current loss 0.022 W and hysteresis loss 0.060 W, which means that no additional cooling costs are incurred.

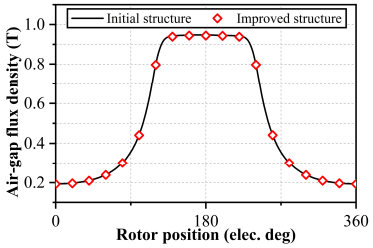

Fig. 15. The no-load air-gap magnetic flux density.

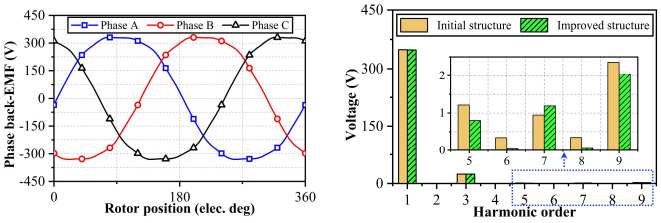

Fig. 16. Voltage. (a) Three-phase no-load back-EMF waveform of the improved structure. (b) Spectrum of the voltage under the rated load condition.

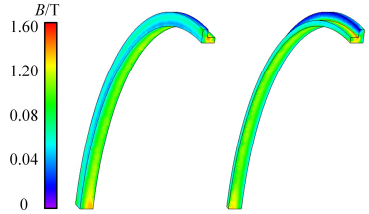

Fig. 17. Flux density distribution of L-shaped flux diverter in generating operation.

V. CONCLUSION

In this paper, considering the critical current reduction of local turn caused by uneven distribution of external magnetic field, the HTS coil in a 10 kW HTS-HIM is designed on purpose to ensure the safety of HTS-HIM and maximize the performance of HTS coil. First, the design process of HTS-HIM is described, including EM and HTS coil design. The design of HTS coil is based on the excitation MMF and parameters of excitation window obtained from EM design. Second, the feasibility and efficiency of using constant sweep rate method to calculate critical current in the design stage of HTS coil are analyzed. The recommended sweep rate and simulation step size are 1 A/s and 0.1 s, respectively. Taking into account the critical current reduction of local turn of HTS coil, the excitation current and number of turns are determined. Third, to improve the analysis efficiency, a 2D axisymmetric direct coupling FEA model of HTS-HIM is established. The results of field analysis show that the innermost turns at the two ends have the smallest critical current. Based on the external field distribution, an easy installed L-shaped flux diverter is proposed to suppress the critical current reduction of local turn of HTS coil. The proposed L-shaped flux diverter increases the current safety margin by 24 % with 0.125 kg weight and 0.082 W iron loss. It does not significantly increase HTS-HIM weight and cooling costs. Moreover, the relative difference of the ideal and actual critical currents is reduced by 35.9 %.

Although this paper focuses on the HTS-HIM, the design method described and the principle of suppressing the critical current reduction of local turn of HTS coil are also applicable to other superconducting machines.

REFERENCES

[1] D. Dezhin, N. Ivanov, K. Kovalev, I. Kobzeva, and V. Semenihin, "System Approach of Usability of HTS Electrical Machines in Future Electric Aircraft", *IEEE Trans. Appl. Supercond.*, vol. 28, no. 4, pp. 1–5, Jun. 2018.

[2] K. S. Haran *et al.*, "High power density superconducting rotating machines—development status and technology roadmap", *Supercond. Sci. Technol.*, vol. 30, no. 12, p. 123002, Dec. 2017.

[3] C. C. T. Chow, M. D. Ainslie, and K. T. Chau, "High temperature superconducting rotating electrical machines: An overview", *Energy Rep.*, vol. 9, pp. 1124–1156, Dec. 2023.

[4] J. Yang, P. Liu, C. Ye, L. Wang, X. Zhang, and S. Huang, "Multidisciplinary Design of High-Speed Solid Rotor Homopolar Inductor Machine for Flywheel Energy Storage System", *IEEE Trans. Transp. Electrification*, vol. 7, no. 2, pp. 485–496, Jun. 2021.

[5] Y. J. Hwang, J. Y. Jang, and H. Jeon, "Overhang Effect Analysis of a Homopolar HTS Synchronous Generator Using 3D Finite Element Method", *IEEE Trans. Appl. Supercond.*, vol. 30, no. 4, pp. 1–5, Jun. 2020.

[6] J.-S. Jeong, D. An, J.-P. Hong, H.-J. Kim, and Y.-S. Jo, "Design of a 10-MW-Class HTS Homopolar Generator for Wind Turbines", *IEEE Trans. Appl. Supercond.*, vol. 27, no. 4, pp. 1–4, Jun. 2017.

[7] K. Sivasubramaniam, E. T. Laskaris, M. R. Shah, J. W. Bray, and N. R. Garrigan, "High-Temperature Superconducting Homopolar Inductor Alternator for Marine Applications", *IEEE Trans. Appl. Supercond.*, vol. 18, no. 1, pp. 1–6, Mar. 2008.

[8] M. Lokhandwalla, K. S. Haran, and J. P. Alexander, "Scaling studies of high speed high temperature superconducting generator", in *2012 XXth International Conference on Electrical Machines*, Marseille, France, Sep. 2012, pp. 751–756.

[9] S. Kalsi, K. Hamilton, R. Buckley, and R. Badcock, "Superconducting AC Homopolar Machines for High-Speed Applications", *Energies*, vol. 12, no. 1, p. 86, Dec. 2018.

[10] K. Sivasubramaniam *et al.*, "Development of a high speed multi-megawatt HTS generator for airborne applications", in *2008 IEEE Power and Energy Society General Meeting - Conversion and Delivery of Electrical Energy in the 21st Century*, Pittsburgh, PA, USA, Jul. 2008, pp. 1–4.

[11] W. Li, K. T. Chau, T. W. Ching, Y. Wang, and M. Chen, "Design of a High-speed Superconducting Bearingless Machine for Flywheel Energy Storage Systems", *IEEE Trans. Appl. Supercond.*, pp. 1–1, 2014.

[12] S. Wang, W. Yang, A. Tian, D. Song, and M. Bai, "Electromagnetic performance analysis of superconducting hybrid excitation homopolar inductor alternator", in *2021 IEEE Sustainable Power and Energy Conference (iSPEC)*, Nanjing, China, Dec. 2021, pp. 3598–3604.

[13] J. Glowacki, Y. Sun, J. G. Storey, T. Huang, R. Badcock, and Z. Jiang, "Temperature Distribution in the Field Coil of a 500-kW HTS AC Homopolar Motor", *IEEE Trans. Appl. Supercond.*, vol. 32, no. 1, pp. 1–8, Jan. 2022.

[14] J. Ma *et al.*, "Design of a 10kW Superconducting Homopolar Inductor Machine Based on HTS REBCO Magnet", *IEEE Trans. Appl. Supercond.*, pp. 1–6, 2023.

[15] Y. Liu *et al.*, "Comparison of 2D simulation models to estimate the critical current of a coated superconducting coil", *Supercond. Sci. Technol.*, vol. 32, no. 1, p. 014001, Jan. 2019.

[16] V. Zermeño, F. Sirois, M. Takayasu, M. Vojenciak, A. Kario, and F. Grilli, "A self-consistent model for estimating the critical current of superconducting devices", *Supercond. Sci. Technol.*, vol. 28, no. 8, p. 085004, Aug. 2015.

[17] F. Gömöry, "Probability of Premature Quenching of HTS Coil Due to Local Reduction of Critical Current", *IEEE Trans. Appl. Supercond.*, vol. 32, no. 6, pp. 1–5, Sep. 2022.

[18] J.-X. Jin, X.-Y. Chen, X.-D. Liu, Z.-H. Chen, and J.-G. Peng, "Influence of Flux Diverter on Energy Storage Property of Small SMES Magnet Wound by 100-m-Class GdBCO Tape", *IEEE Trans. Appl. Supercond.*, vol. 28, no. 4, pp. 1–5, Jun. 2018.

[19] S. Song *et al.*, "Analysis of the Notch Effect on Flux Diverters for High-Temperature Superconducting Magnets", *IEEE Trans. Appl. Supercond.*, vol. 26, no. 4, pp. 1–4, Jun. 2016.

[20] Y. Zhang, Y. Cheng, R. Qu, D. Li, Y. Gao, and Q. Wang, "AC Loss Analysis and Modular Cryostat Design of a 10-MW High-Temperature Superconducting Double Stator Flux Modulation Machine", *IEEE Trans. Ind. Appl.*, vol. 58, no. 6, pp. 7153–7162, Nov. 2022.

[21] Y. Pan, J. Yang, Q. Li, X. Luo, S. Huang, and J. Ma, "Optimal Design of a High Temperature Superconducting Homopolar Inductor Machine", in *2023 26th International Conference on Electrical Machines and Systems (ICEMS)*, Nov. 2023, pp. 3920–3925.

[22] J. Yang *et al.*, "Investigation on the Method for Reducing the Time Constant of Exciting Winding of Homopolar Inductor Machine", *IEEE Trans. Transp. Electrification*, vol. 9, no. 2, pp. 3255–3267, Jun. 2023.

[23] F. Huber, W. Song, M. Zhang, and F. Grilli, "The T-A formulation: an efficient approach to model the macroscopic electromagnetic behaviour of HTS coated conductor applications", *Supercond. Sci. Technol.*, vol. 35, no. 4, p. 043003, Apr. 2022.

[24] E. Berrospe-Juarez, F. Trillaud, V. M. R. Zermeño, and F. Grilli, "Advanced electromagnetic modeling of large-scale high-temperature superconductor systems based on H and T-A formulations", *Supercond. Sci. Technol.*, vol. 34, no. 4, p. 044002, Apr. 2021.

[25] H. Zhang, M. Zhang, and W. Yuan, "An efficient 3D finite element method model based on the *T–A* formulation for superconducting coated conductors", *Supercond. Sci. Technol.*, vol. 30, no. 2, p. 024005, Feb. 2017.

[26] "Robinson HTS Wire Critical Current Database". Robinson Research Institute, 2022. Available: htsdb.wimbush.eu.

[27] Y. Pan, J. Yang, X. Luo, H. Xiao, and J. Ma, "A Method for Calculating Critical Current of High Temperature Superconducting Machine Based on Magnetic Vector Potential", *IEEE Trans. Appl. Supercond.*, pp. 1–6, 2024.

[28] C. Hartmann, R. Mellerud, J. K. Nøland, and R. Nilssen, "A Static FEA Framework for Fast Analysis of HTS Armature Windings in AC Superconducting SMPM Machines", *IEEE Trans. Energy Convers.*, pp. 1–11, 2023.

[29] J. Yang *et al.*, "Analysis of the Electromagnetic Performance of Homopolar Inductor Machine Through Nonlinear Magnetic Equivalent Circuit and Air-Gap Permeance Function", *IEEE Trans. Ind. Appl.*, vol. 56, no. 1, pp. 267–276, Jan. 2020.

[30] T. Benkel *et al.*, "*T–A* -Formulation to Model Electrical Machines With HTS Coated Conductor Coils", *IEEE Trans. Appl. Supercond.*, vol. 30, no. 6, pp. 1–7, Sep. 2020.

Yuanhang Pan received the B.Eng. degree in electrical engineering from the Wuhan University of Technology, Wuhan, China, in 2022. He is currently working toward the M.S. degree in electrical engineering with the College of Electrical and Information Engineering, Hunan University, Changsha, China.

His research interests include the design and analysis of homopolar inductor machines, superconducting machines and high-speed electrical machines.

Jiangtao Yang received the B.Eng. degree in electrical engineering from the Wuhan University of Technology, Wuhan, China, in 2014 and the Ph.D. degree in electrical engineering from the Huazhong University of Science and Technology, Wuhan, China, in 2019. He is currently an Associate Professor with the College of Electrical and Information Engineering, Hunan University, Changsha, China.

His research interests include the design and analysis of high-speed electrical machines, pulsed alternators, and flywheel energy storage systems.

Qing Li received the B.Eng. degree in electrical engineering from Southwest University, Chongqing, China, in 2021. He is

currently working toward the Ph.D. degree in electrical engineering from Hunan University, Changsha, China.

His research interests include the design and analysis of permanent magnet motors, homopolar inductor machines, and flywheel energy storage systems.

Shoudao Huang received the B.Eng. and Ph.D. degrees in electrical engineering from the College of Electrical and Information Engineering, Hunan University, Changsha, China, in 1983, and 2005, respectively. He is currently a Full-Time Professor with the College of Electrical and Information Engineering, Hunan University.

His research interests include motor design and control, power electronic system and control, and wind energy conversion systems.

Xuezhi Luo received the master's degree in power engineering from the North China Electric Power University, Baoding, China, in 2021. He is currently pursuing the Ph.D. degree in electrical engineering with the College of Electrical and Information Engineering, Hunan University, Changsha, China.

His research interests include the design and analysis of superconducting magnets, superconducting windings and superconducting electrical machines.

Chuang Gao received the B.S. degree in mechanical engineering from the Jiangsu University of Science and Technology, Zhenjiang, China, in 2003, and the Ph.D. degree in fluid machinery from Shanghai Jiao Tong University, Shanghai, China, in 2010.

Since 2010, he has been an Associate Professor with the Shanghai Advanced Research Institute, Chinese Academy of Sciences, Shanghai. He has authored more than 20 articles and holds more than 15 inventions. His research interests include aerodynamics of radial turbomachinery, rotor dynamics, and high-speed generators.

Jun Ma received B.S. degree in electrical engineering and automation from Zhejiang University, Hangzhou, China, in 2013, and the M.S. degree in electrical engineering from Shanghai Jiao Tong University, Shanghai, China, in 2016, and the Ph.D. degree in electrical engineering from the University of Cambridge, Cambridge, U.K. in 2020. In 2022, he was an Associate Professor with Hunan University, Changsha, China.

Since 2022, he has been a Lecturer/Assistant Professor in electrical engineering with the University of Bristol, Bristol, U.K. His research interests include high-temperature superconductors.